

References and Notes

1. Y. Yokoyama, K. Lambeck, P. De Deckker, P. Johnston, L. K. Fifield, *Nature* **406**, 713 (2000).
2. S. Manabe, R. J. Stouffer, *Paleoceanography* **12**, 321 (1997).
3. A. F. Fanning, A. J. Weaver, *Paleoceanography* **12**, 307 (1997).
4. I. Shennan, G. A. Milne, *Quat. Sci. Rev.* **22**, 1543 (2003).
5. D. Q. Bowen, F. M. Phillips, A. M. McCabe, P. C. Knutz, G. A. Sykes, *Quat. Sci. Rev.* **21**, 89 (2002).
6. P. M. Grootes, M. Stuiver, J. W. C. White, S. Johnsen, J. Jouzel, *Nature* **366**, 552 (1993).
7. E. Bard, F. Rostek, J.-L. Turon, S. Gendreau, *Science* **289**, 1321 (2000).
8. A. Schmittner, M. Yoshimori, A. J. Weaver, *Science* **295**, 1489 (2002).
9. A. M. McCabe, P. U. Clark, *Nature* **392**, 373 (1998).
10. The cut-and-fill nature of the channels suggests an erosional phase followed by a depositional phase, and the orientation of the channel axes suggests erosion by easterly flowing water draining the adjacent Mourné Mountains. We exclude a subglacial origin for the channels because they are eroded into glaciomarine sediments that were deposited subaqueously. The orientation of the channel axes perpendicular to the coast indicates that if the channels were eroded subaqueously during high relative sea level by a continuation of easterly flowing streams draining the adjacent Mourné Mountains, then there should be deltas deposited by these streams at the contemporaneous sea level. The absence of any such deltas, however, leads us to dismiss this possibility. We also exclude a subaqueous origin because there is no a priori reason why subaqueous processes would initially be erosional, followed by a switch to processes that result in nearly instantaneous infilling of the channels by sediments, particularly on low slopes and at shallow water depths (<30 m). We thus argue that a subaerial origin best explains the erosional phase, which we interpret as having occurred after initial deglaciation of the Kilkeel coast and subsequent isostatic emergence. Subsequent rapid deposition of marine sediments in the channels thus requires a rapid rise in eustatic sea level to flood the channels on what was otherwise still an isostatically emergent coast. The timing of local deglaciation (5) and the formation of the associated marine limit relative to the timing of channel filling (19,000 years B.P.) provides sufficient time for coastal emergence and subaerial channel erosion to occur.
11. The radiocarbon-dated fossil microfauna are dominated by the foraminifer *E. clavatum* (>90%) and the ostracod *Roundstonia globulifera* (5 to 10%). All foraminiferal tests are glassy and in pristine condition, including preservation of delicate ornamentation and of the last aperture. Valves of *R. globulifera* show intact instars, and valves of *Polycopse* sp. are still attached.
12. Assuming a reservoir age correction of 400 years, our five radiocarbon ages have the same weighted mean ¹⁴C age (16,640 ± 40 ¹⁴C years B.P.) (at 2σ) as the weighted mean of three ¹⁴C ages (16,360 ± 220 ¹⁴C years B.P.) on a single sample of Barbados coral that has a corresponding weighted mean U/Th age of 19,000 ± 70 years B.P. (14). A larger reservoir age correction applied to our samples would improve this agreement. Independent calendar age constraints indicate that the reservoir age of North Atlantic surface waters increased substantially during cold periods of the last glaciation (34). On the basis of lower-end estimates of reservoir ages for the Younger Dryas (820 years) and H1 (1230 years) (34), we thus assume that a reservoir age of 1000 ± 200 years applies to the Oldest Dryas cold period initiated by the 19-ky MWV, and we calibrate our samples accordingly.
13. C. Hillaire-Marcel, A. de Vernal, G. Bilodeau, A. J. Weaver, *Nature* **410**, 1073 (2001).
14. E. Bard, M. Arnold, B. Hamelin, N. Tisnerat-Laborde, G. Cabioch, *Radiocarbon* **40**, 1085 (1998).
15. K. A. Hughen, J. R. Southon, S. J. Lehman, J. T. Overpeck, *Science* **290**, 1951 (2000).
16. J. C. Duplessy et al., *Paleoceanography* **3**, 343 (1988).

17. A. J. Weaver, M. Eby, A. F. Fanning, E. C. Wiebe, *Nature* **394**, 847 (1998).
18. R. Zahn et al., *Paleoceanography* **12**, 696 (1997).
19. G. Bond et al., *Science* **278**, 1257 (1997).
20. M. Elliot, L. Labeyrie, T. Dokken, S. Manthe, *Earth Planet. Sci. Lett.* **194**, 151 (2001).
21. T. S. Stocker, D. G. Wright, W. S. Broecker, *Paleoceanography* **7**, 529 (1992).
22. A. Schmittner, O. Saenko, A. J. Weaver, *Quat. Sci. Rev.* **22**, 659 (2003).
23. E. Monnin et al., *Science* **291**, 112 (2001).
24. D. F. Gu, S. G. H. Philander, *Science* **275**, 805 (1997).
25. A. J. Weaver, *Geophys. Res. Lett.* **26**, 743 (1999).
26. Z. Liu et al., *Geophys. Res. Lett.* **29** (10), 10.1029/2001GL013938 (2002).
27. M. Feldberg, A. C. Mix, *Paleoceanography* **18** (1), 10.1029/2001PA000740 (2003).
28. J. R. Toggweiler, K. Dixon, W. S. Broecker, *J. Geophys. Res.* **96**, 20 (1991).
29. H. J. Spero, D. W. Lea, *Science* **296**, 522 (2002).
30. D. M. Sigman, E. A. Boyle, *Nature* **407**, 859 (2000).
31. M. R. Palmer, P. N. Pearson, *Science* **300**, 480 (2003).
32. A. J. Weaver, O. Saenko, P. U. Clark, J. X. Mitrovica, *Science* **299**, 1709 (2003).
33. T. Hanebuth, K. Statterger, P. M. Grootes, *Science* **288**, 1033 (2000).
34. C. Waelbroeck et al., *Nature* **412**, 724 (2001).
35. A. C. Mix et al., in *Mechanisms of Global Climate*

Change at Millennial Time Scales, P. U. Clark, R. S. Webb, L. D. Keigwin, Eds., vol. 112 of *Geophysical Monographs* (American Geophysical Union, Washington, DC, 1999), pp. 127–148.

36. R. Zahn et al., *Paleoceanography* **12**, 696 (1997).
37. M. Stuiver, P. M. Grootes, *Quat. Res.* **53**, 277 (2000).
38. C. Rühlemann, S. Mulitza, P. J. Muller, G. Wefer, R. Zahn, *Nature* **402**, 511 (1999).
39. A. Shemesh et al., *Paleoceanography* **17** (4), 10.1029/2000PA000599 (2002).
40. S. J. Johnsen, W. Dansgaard, H. B. Clausen, C. C. Langway, *Nature* **235**, 429 (1972).
41. T. Blunier, E. J. Brook, *Science* **291**, 109 (2001).
42. A. Berger, M. F. Loutre, *Quat. Sci. Rev.* **10**, 297 (1991).
43. K. Visser, R. Thunell, L. Stott, *Nature* **421**, 152 (2003).
44. W. H. Berger, J. S. Killingley, *Mar. Geol.* **45**, 93 (1982).
45. M. G. Dinkelman, thesis, Oregon State University (1974).
46. We thank T. Guilderson and C. Bryant for providing AMS radiocarbon ages, and D. Bowen, S. Hostetler, and N. Pias for helpful discussions. Supported by the University of Ulster (P.U.C. and A.M.M.), the NSF Earth System History program (P.U.C.) and Marine Geology and Geophysics program (A.C.M.), and the Canadian Natural Sciences and Engineering Research Council, the Killam Foundation, and the Canada Research Chair program (A.J.W.).

8 December 2003; accepted 16 April 2004

Wind as a Long-Distance Dispersal Vehicle in the Southern Hemisphere

Jesús Muñoz,^{1*} Ángel M. Felicísimo,² Francisco Cabezas,¹ Ana R. Burgaz,³ Isabel Martínez⁴

Anisotropic (direction-dependent) long-distance dispersal (LDD) by wind has been invoked to explain the strong floristic affinities shared among landmasses in the Southern Hemisphere. Its contribution has not yet been systematically tested because of the previous lack of global data on winds. We used global winds coverage from the National Aeronautics and Space Administration SeaWinds scatterometer to test whether floristic similarities of Southern Hemisphere moss, liverwort, lichen, and pteridophyte floras conform better with (i) the anisotropic LDD hypothesis, which predicts that connection by "wind highways" increases floristic similarities, or (ii) a direction-independent LDD hypothesis, which predicts that floristic similarities among sites increase with geographic proximity. We found a stronger correlation of floristic similarities with wind connectivity than with geographic proximities, which supports the idea that wind is a dispersal vehicle for many organisms in the Southern Hemisphere.

Dispersal mechanisms play a key role in determining plant and animal distributions. LDD, defined as passive transport by wind, storms, water flows, and other means (1), was proposed as early as 1845 (2) and is often invoked to explain biotic similarities between distant landmasses (3–6). However, some authors have questioned the likelihood of LDD by wind because it is so

difficult to support the theory with experimental data (7, 8).

Here, we tested whether the shared floristic affinities among extratropical Southern Hemisphere landmasses can be explained by LDD of propagules by wind. We used data from the SeaWinds scatterometer (on board the QuikSCAT satellite) to model wind connectivity among landmasses and to test how well these wind highways explain the floristic similarities observed in four groups of cryptogams (mosses, liverworts, lichens, and pteridophytes). All four have both sexual and asexual propagules suitable for LDD, although the relative importance of each mode varies among the groups. The hypothesis that floristic similarities are due to wind dispersal

¹Real Jardín Botánico, Plaza de Murillo 2, 28014 Madrid, Spain. ²Escuela Politécnica, Universidad de Extremadura, 10071 Cáceres, Spain. ³Departamento de Biología Vegetal I, Universidad Complutense, 28040 Madrid, Spain. ⁴Ciencias Experimentales y Tecnología, Universidad Rey Juan Carlos, 28933 Móstoles, Spain.

*To whom correspondence should be addressed. E-mail: jmunoz@ma-rjb.csic.es

implies an anisotropic (direction-dependent) transport along wind highways defined by wind azimuth and speed. We compared this hypothesis with the neutral hypothesis (9), in which floristic similarities are better explained by isotropic (direction-independent) transport and thus depend only on geographic proximity.

To test how well the floristic affinities among extratropical Southern Hemisphere landmasses agree with the two proposed hypotheses, we recorded plant data for the 27 localities shown in Fig. 1. There are four data sets: mosses (601 species), liverworts (461 species), lichens (597 species), and pteridophytes (192 species), totaling 1851 species (tables S1 to S4). Only species shared by at least two localities were included. The Ochiai index (10) was used to calculate the four floristic similarity matrices. The wind connectivity matrices were generated from SeaWinds scatterometer data for the period from June 1999, when SeaWinds began operating, to March 2003. SeaWinds provides near-global daily measurements of wind azimuth and speed over the ocean surface at a spatial resolution of 25 km (11, 12). Data were aggregated into 10-day syntheses and reprojected onto a universal polar stereographic to eliminate blanks in satellite coverage and topologic discontinuities. We produced a set of 139 map pairs representing the evolution of wind azimuth and speed during the study period. From these maps, the resistance of traveling between each locality pair with wind as a vehicle (351 combinations) was calculated for all of the 10-day periods. The result is a set of 139 matrices of wind connectivity values, or the complement of resistance (Fig. 1). Finally, we calculated pairwise great circle distances between all localities in the study (for the complete data set, see database S1).

To test the two hypotheses, we first used Mantel tests. As a second and statistically independent analysis, we used multidimensional scaling to generate three-dimensional maps for floristic similarities, maximum annual wind connectivity, and geographic proximities. The pairwise fit among configurations was evaluated by a Procrustes analysis (10).

Mantel tests show a highly significant correlation of the four floristic similarities with both wind connectivity and geographic proximity, which are each highly collinear (table S5). Correlation coefficient time series in Fig. 2 show a clear seasonal pattern for mosses, liverworts, and lichens, with lower correlation values corresponding to periods of about 100 days in austral spring. The cause could be the growth of ice over sub-Antarctic waters, which prevents SeaWinds data capture and consequently generates null wind connectivity values for the frozen sites (because no

pteridophytes grow in the landmasses covered by ice during austral spring, there are no drops for this group).

To distinguish the relative importance of geographic proximity and wind connectivity, it is necessary to determine whether the correlation of geographic proximity with floristic similarity is as high inside the wind highways as it is outside them. If wind is the dispersal vehicle, correlations among sites at similar distances will be higher inside wind highways and lower outside. We have checked this assumption by searching for sites with low floristic similarities that are close in space but not connected by wind and, conversely, for sites with high floristic similarities that are

distant but connected by wind highways. The view that wind is a dispersal vehicle is supported by cases like Macquarie Island [locality (loc.) 24, Fig. 1], which has a higher floristic similarity with the remote Juan Fernandez [loc. 1; 8780 km; mosses floristic similarity (fs) = 0.241; liverworts fs = 0.133; lichens fs = 0.110; and pteridophytes fs = 0.158] and Tierra del Fuego (loc. 2; 7550 km; mosses fs = 0.320; liverworts fs = 0.146; lichens fs = 0.300; and pteridophytes fs = 0.233) than with the closer Lord Howe (loc. 21; 2565 km; mosses fs = 0.183; liverworts fs = 0.000; lichens fs = 0.110; and pteridophytes fs = 0.000), Norfolk (loc. 23; 2935 km; mosses fs = 0.140; liverworts fs = 0.152; lichens

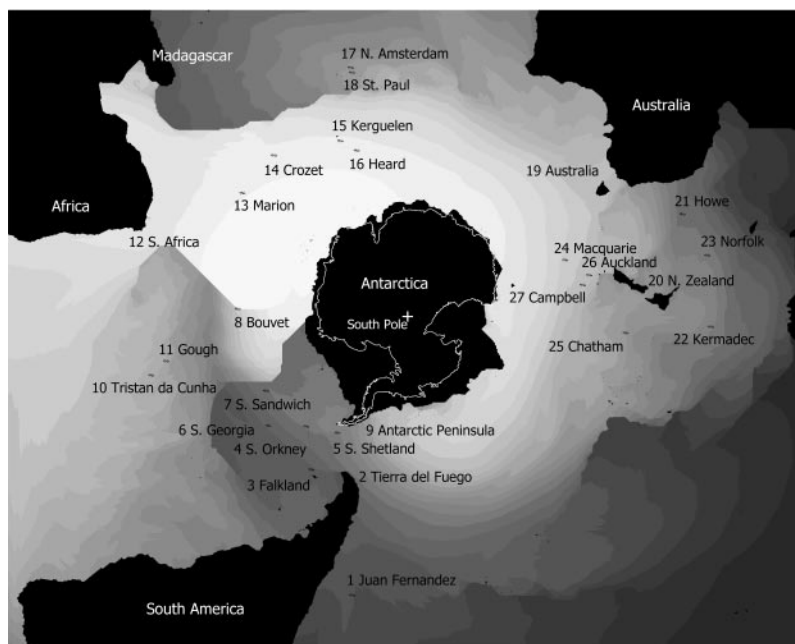


Fig. 1. Universal polar stereographic map of the study area with the 27 localities treated. Gray tones represent wind connectivity for Bouvet Island (loc. 8) for the period from 1 to 10 February 2002 (increasing connectivity from dark to pale in the range 0 to 1, adimensional). Wind connectivity is the complement of the resistance of traveling between two points with wind as a vehicle and was estimated from SeaWinds scatterometer measurements. Because SeaWinds only records wind properties over ocean water surface, landmasses and ocean surface covered with ice, as well as areas with null connectivity values for this period, appear black in the figure because of the absence of data. Wind connectivity values were calculated by anisotropic cost analysis (supporting online material text), which assigns a minimum resistance to the movement in the exact wind vector azimuth and incrementally penalizes angular deviations. Similarly, higher speed values diminish resistance and thereby increase connectivity.

Table 1. Pearson correlation coefficient of floristic similarities with maximum annual wind connectivity and geographic proximity as measured with simple Mantel tests. Maximum wind connectivity values are the highest for each site pair in the given year. All correlations are statistically significant ($P < 0.001$) as determined by a Monte Carlo permutation test that examined 999 replicates.

Year	Maximum wind connectivity					Geographic proximity
	1999	2000	2001	2002	2003	
Mosses (601 species)	0.594	0.601	0.602	0.588	0.617	0.579
Liverworts (461 species)	0.515	0.515	0.525	0.504	0.505	0.460
Lichens (597 species)	0.514	0.508	0.407	0.415	0.509	0.492
Pteridophytes (192 species)	0.573	0.549	0.551	0.535	0.553	0.543

REPORTS

$f_s = 0.060$; pteridophytes $f_s = 0.000$), or Kermadec (loc. 22; 3280 km; mosses $f_s = 0.160$; liverworts $f_s = 0.071$; lichens $f_s = 0.070$; and pteridophytes $f_s = 0.000$). Another notable example is Bouvet (loc. 8, Fig. 1), which has a higher floristic similarity with the distant Kerguelen (loc. 15; 4420 km; mosses $f_s = 0.262$; liverworts $f_s = 0.091$; lichens $f_s = 0.160$; and pteridophytes, not applicable) and Heard (loc. 16; 4430 km; mosses $f_s = 0.302$; liverworts $f_s = 0.289$; and lichens $f_s = 0.320$) than with the closer Gough (loc. 11; 1860 km; mosses $f_s = 0.162$; liverworts $f_s = 0.177$; and lichens $f_s = 0.000$).

We also attempted to incorporate the fact that dispersal events are episodic rather than gradual (13–16) by testing floristic similarities against maximum annual wind connectivity and geographic proximity. In 85% of the cases (17 out of 20), Mantel tests resulted in higher correlation values with wind connectivity than with geographic proximity (Table 1), supporting the episodic nature of dispersal events.

According to a z -Fisher transformation test, the r values in Table 1 are statistically indistinguishable. However, the probability of obtaining 17 or more Pearson correlation coefficient values of floristic similarities with

maximum annual wind connectivity that are higher than the corresponding Pearson correlation coefficient values of floristic similarities with geographic proximity is less than 0.001, suggesting that values in Table 1 are not random. Moreover, the second, and independent, statistical analysis helped to unravel the relative contribution of wind and geographic proximity to explain the present floristic affinities. Multidimensional scaling with the use of the PROXSCAL algorithm (17) was performed to generate the minimum S-stress spatial configurations from floristic similarities, maximum annual wind connectivity, and geographic proximities data. Later, we performed a Procrustes analysis to compare the fit between the configuration derived from floristic similarities and every other spatial configuration. To test the statistical significance of the fits, we used the randomization method PROTEST (18).

Results in Table 2 show that mosses, liverworts, and lichens have a stronger association of floristic similarities with maximum wind connectivity than with geographic proximity, which supports the hypothesis that winds are the main force driving current plant distributions. However, for pteridophytes, the association is about equal with both variables, indicating that most pteridophytes, although dispersed by wind (19), have a limitation in the maximum distance of dispersal. This difference is in agreement with what can be expected on the basis of extratropical pteridophyte dispersal peculiarities with regard to the other groups studied. Whereas asexual propagules (fragments of mature individuals, special reproductive bodies like gemmae, soralia, or isidia) may play the central role in the dispersion of mosses, liverworts, and lichens (20–25), their importance is likely negligible in extratropical pteridophytes. In addition, the foundation of a colony by spores imposes the following more stringent constraints on pteridophytes than on the other groups (26): (i) For species with only green spores, viability and tolerance to travel in wind currents are lower than for species with nongreen spores, and (ii) although foundation from a single spore has been documented, it must be followed by intragametophytic selfing to establish a viable colony.

The groups we studied are phylogenetically remote and heterogeneous in their transport and establishing requirements. The same dispersal mechanism should work for other organisms suitable to wind transport in lower atmospheric layers, such as arthropods, fungi, or angiosperms with small propagules (e.g., orchids). Further research should extend this study to such groups and also introduce molecular data to test whether genetic similarities between areas also show a high correla-

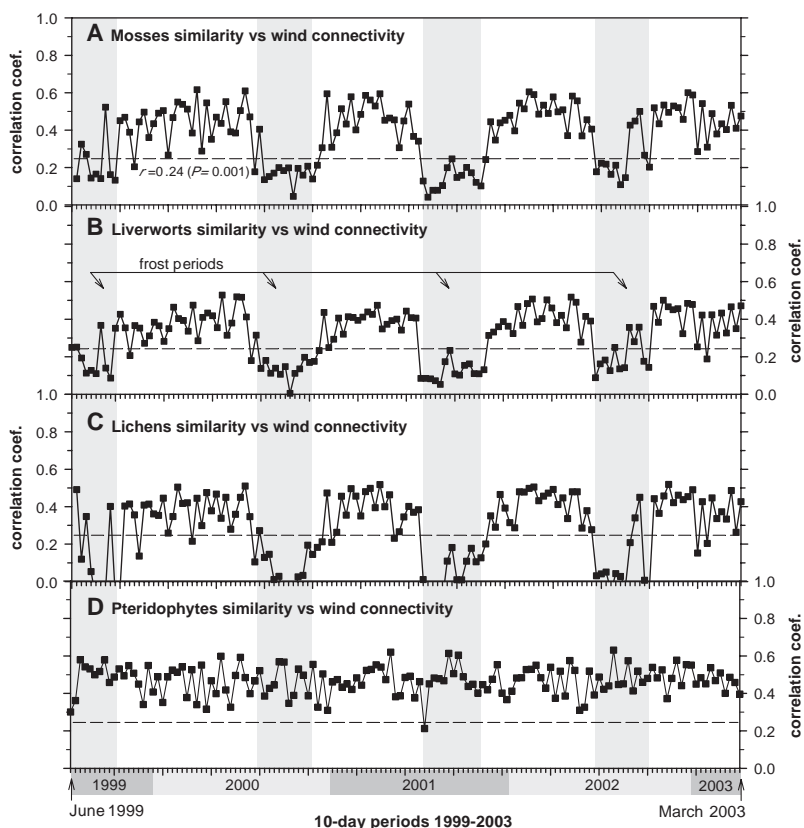


Fig. 2. Pearson correlation coefficients of floristic similarities with wind connectivity for the four groups as measured with Mantel tests. Time series show a clear seasonality in moss (A), liverwort (B), and lichen (C) series, with drops that may be the result of propagule inaccessibility or data blanks owing to ice coverage. This pattern is not evident in the pteridophyte series (D) because no member of this group grows in landmasses seasonally covered by ice. coef., coefficient.

Table 2. Fit significance (P values for m^2 Procrustes statistic) between floristic similarity, maximum annual wind connectivity, and geographic proximity spatial configurations. The configurations were obtained with multidimensional scaling with the use of the PROXSCAL algorithm, and the fits and their significance were calculated by Procrustes analysis and a randomization test that examined 10,000 replicates with the PROTEST method.

Year	Maximum wind connectivity					Geographic proximity
	1999	2000	2001	2002	2003	
Mosses (601 species)	0.007	0.023	0.032	0.004	0.008	0.112
Liverworts (461 species)	0.004	0.007	0.018	0.009	0.043	0.062
Lichens (597 species)	0.003	0.110	0.118	0.004	0.013	0.260
Pteridophytes (192 species)	0.004	0.005	0.012	0.003	0.010	0.003

tion with wind connectivity, which would independently validate our hypothesis.

References and Notes

- N. Shigesada, K. Kawasaki, in *Dispersal Ecology*, J. M. Bullock, R. E. Kenward, R. S. Hails, Eds. (Blackwell, Malden, UK, 2002), pp. 350–373.
- J. D. Hooker, *The Botany of the Antarctic Voyage, Vol. 1: Flora Antarctica* (Reeve, London, 1845).
- W. R. B. Oliver, *J. Linn. Soc. Bot.* **47**, 99 (1925).
- J. A. Freeman, *J. Anim. Ecol.* **14**, 128 (1945).
- P. H. Raven, *N.Z. J. Bot.* **11**, 177 (1973).
- R. C. Winkworth, S. J. Wagstaff, D. Glenny, P. J. Lockhart, *Trends Ecol. Evol.* **17**, 514 (2002).
- J. J. Morrone, J. Crisci, *Annu. Rev. Ecol. Syst.* **26**, 373 (1995).
- C. J. Humphries, L. R. Parenti, *Cladistic Biogeography: Interpreting Patterns of Plant and Animal Distributions* (Oxford Univ. Press, Oxford, ed. 2, 1999).
- S. P. Hubbell, *The Unified Neutral Theory of Biodiversity and Biogeography* (Princeton Univ. Press, Princeton, NJ, 2001).
- P. Legendre, L. Legendre, *Numerical Ecology* (Elsevier, Amsterdam, 1998).
- Additional information about the SeaWinds scatterometer on the QuikSCAT satellite is available at <http://podaac.jpl.nasa.gov/quikscat>.
- Jet Propulsion Laboratory, *SeaWinds on QuikSCAT Level 3: Daily, Gridded Ocean Wind Vectors (JPL SeaWinds Project), Guide Document Version 1.1* (California Institute of Technology, CA, 2001).
- R. C. Close, N. T. Moar, A. I. Tomlinson, A. D. Lowe, *Int. J. Biometeorol.* **22**, 1 (1978).
- W. A. Marshall, *Nature* **383**, 680 (1996).
- P. Greenslade, R. A. Farrow, J. M. B. Smith, *J. Biogeogr.* **26**, 1161 (1999).
- K. Sassen et al., *J. Atmos. Sci.* **60**, 873 (2003).
- Additional information about the PROXSCAL algorithm is available at <http://egasmoniz.edu.pt/nesia/documentacao/formulas/proxscal.pdf>.
- D. A. Jackson, *Ecoscience* **2**, 297 (1995).
- H. Tuomisto, K. Ruokolainen, M. Yli-Halla, *Science* **299**, 241 (2003).
- B. O. van Zanten, *J. Hattori Bot. Lab.* **41**, 133 (1976).
- B. O. van Zanten, *J. Hattori Bot. Lab.* **44**, 455 (1978).
- B. O. van Zanten, T. Pócs, *Adv. Bryol.* **1**, 479 (1981).
- N. G. Miller, L. J. H. Ambrose, *Bryologist* **79**, 55 (1976).
- N. G. Miller, *Monogr. Syst. Bot. Missouri Bot. Gard.* **11**, 71 (1985).
- I. M. Brodo, S. D. Sharnoff, S. Sharnoff, *Lichens of North America* (Yale Univ. Press, New Haven, CT, 2001).
- R. Tryon, *Bot. Rev.* **52**, 117 (1986).
- We thank the NASA QuikSCAT team for making data available; J. J. Engel, A. J. Fife, and D. Glenny for providing information about plant distributions; A. Herrero for extensive comments and discussion on the pteridophyte results; and E. Real, L. Barrios, and T. Villagarcía for statistical advice. J.M. conceived the study and generated floristic data on mosses and liverworts; A.M.F. produced GIS models; F.C. generated the pteridophyte data and co-wrote the results on this group; A.R.B. and I.M. generated the lichen data; and J.M. and A.M.F. designed and carried out the statistical analyses and co-wrote the paper. G. Milder (St. Louis) kindly revised the English text.

Supporting Online Material

www.sciencemag.org/cgi/content/full/304/5674/1144/DC1
SOM Text
Tables S1 to S5
References
Database S1

31 December 2003; accepted 16 April 2004

Autoimmune Disease and Impaired Uptake of Apoptotic Cells in MFG-E8-Deficient Mice

Rikinari Hanayama,¹ Masato Tanaka,^{1,4} Kay Miyasaka,^{1,5}
Katsuyuki Aozasa,² Masato Koike,³ Yasuo Uchiyama,³
Shigekazu Nagata^{1,5,6*}

Apoptotic cells expose phosphatidylserine and are swiftly engulfed by macrophages. Milk fat globule epidermal growth factor (EGF) factor 8 (MFG-E8) is a protein that binds to apoptotic cells by recognizing phosphatidylserine and that enhances the engulfment of apoptotic cells by macrophages. We report that tingible body macrophages in the germinal centers of the spleen and lymph nodes strongly express MFG-E8. Many apoptotic lymphocytes were found on the *MFG-E8*^{-/-} tingible body macrophages, but they were not efficiently engulfed. The *MFG-E8*^{-/-} mice developed splenomegaly, with the formation of numerous germinal centers, and suffered from glomerulonephritis as a result of autoantibody production. These data demonstrate that MFG-E8 has a critical role in removing apoptotic B cells in the germinal centers and that its failure can lead to autoimmune diseases.

Apoptosis is a process for removing harmful or useless cells and is fundamental to the maintenance of mammalian homeostasis (1). Apoptotic cells are rapidly engulfed by phagocytes, a process that should prevent inflammation and the autoimmune re-

sponse against intracellular antigens that can be released from the dying cells (2–4). Phosphatidylserine (PS) that is exposed on the surface of apoptotic cells has been identified as a recognition signal for macrophages (5), and several receptors that bind PS have been identified (2, 3). MFG-E8 is secreted from activated macrophages, specifically binds to apoptotic cells by recognizing PS, and enhances the engulfment of apoptotic cells by phagocytes (6).

To examine the in vivo role of MFG-E8, we first examined its expression by Northern blot hybridization (fig. S1). MFG-E8 was strongly expressed in mammary glands (7, 8). Several other tissues such as the spleen, lymph nodes, and brain also expressed MFG-E8 mRNA. Immunohistochemical analysis of spleen sections (9) showed the labeling with

antibody to MFG-E8 in cells localized to germinal centers that were stained by peanut agglutinin (PNA) (Fig. 1). Spleen sections from *MFG-E8*^{-/-} mice (see below) were not stained, which confirmed the specificity of the antibody. Germinal centers contain macrophages called “tingible body” macrophages, which specifically express CD68 but do not express F4/80 (10). Dual staining for MFG-E8 and CD68 or F4/80 showed that the cells expressing MFG-E8 expressed CD68 but did not express F4/80 [Fig. 1, and (11)], which suggests that the tingible body macrophages expressed MFG-E8. The CD68⁺ tingible body macrophages are present not only in the spleen but also in the lymph nodes (10). Staining with antibody against MFG-E8 indicated that the CD68⁺ macrophages in the lymph nodes also expressed MFG-E8 (Fig. 1).

We generated *MFG-E8*^{-/-} mice by gene targeting. The murine *MFG-E8* gene is encoded by 10 exons within 16 kb of genomic DNA on chromosome 7. A targeting vector was constructed by replacing exons 4 to 6 with the *neo*-resistance gene (fig. S2). The vector was introduced into mouse embryonic stem (ES) cells, and ES clones carrying the mutation were identified by polymerase chain reaction (PCR). Mice derived from two ES clones had identical phenotypes, and those from one representative clone were characterized in detail. Thioglycollate activates macrophages (12), and we previously showed that peritoneal macrophages obtained after an intraperitoneal injection of thioglycollate secrete abundant MFG-E8 (6). Accordingly, immunoprecipitation and Western blotting with antibody against MFG-E8 revealed a 74-kD protein in the culture supernatant of thioglycollate-elicited peritoneal macrophages from wild-type mice (Fig. 2A). This

¹Department of Genetics, ²Department of Pathology, and ³Department of Cell Biology and Neuroscience, Osaka University Medical School, 2-2 Yamada-oka, Suita, Osaka 565-0871, Japan. ⁴Laboratory for Innate Cellular Immunity, RIKEN Research Center for Allergy and Immunology, Yokohama, Kanagawa 230-0045, Japan. ⁵Laboratory of Genetics, Integrated Biology Laboratories, Graduate School of Frontier Biosciences, Osaka University, Osaka 565-0871, Japan. ⁶Core Research for Evolutional Science and Technology, Japan Science and Technology Corporation, Osaka 565-0871, Japan.

*To whom correspondence should be addressed. E-mail: nagata@genetic.med.osaka-u.ac.jp.